List of Figures

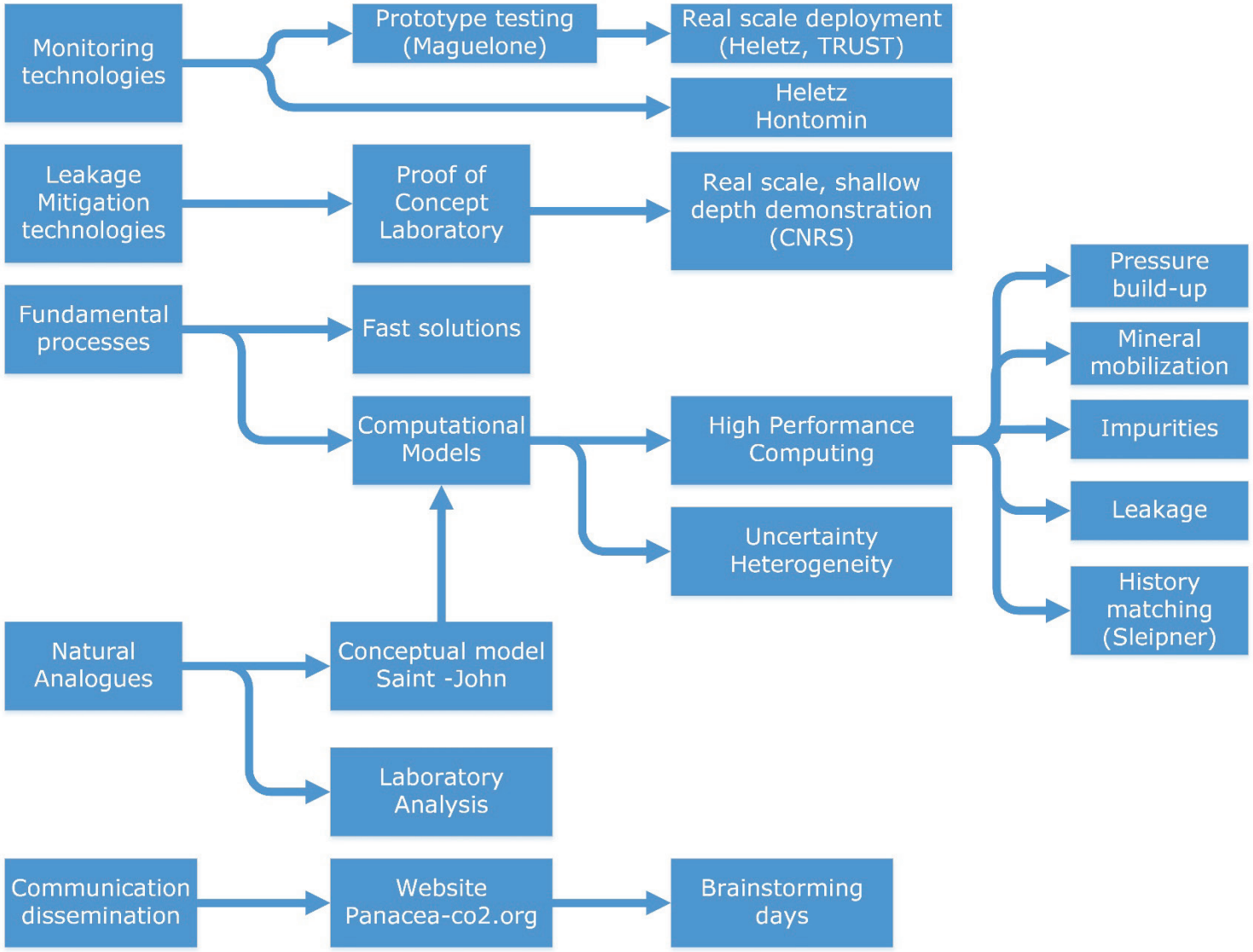

Figure 1: Map to the PANACEA outcome and findings.

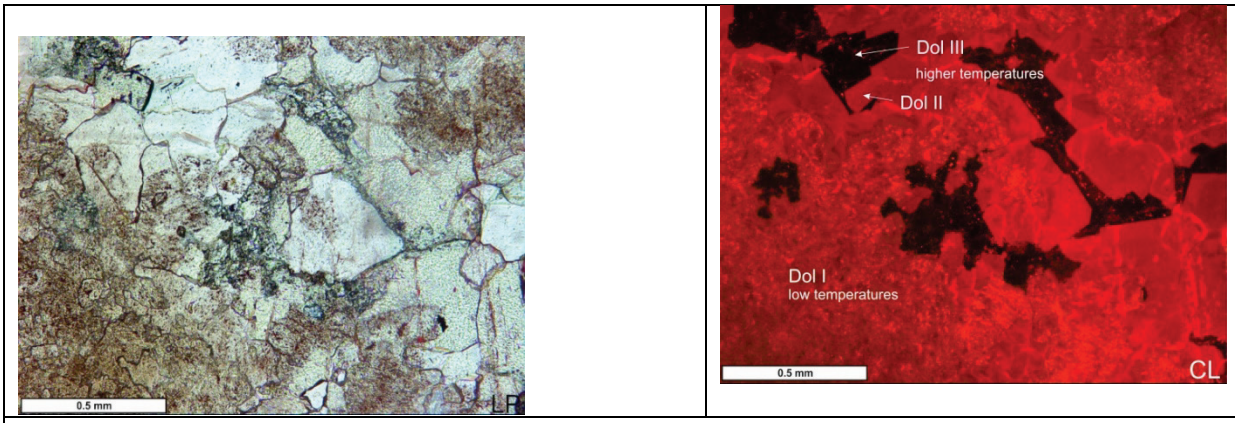

Figure 2: Microphotograph (plane polarized light, left) and cathodoluminescence image (right) illustrating the three different dolomite generations detected along fractures in altered basement granite from below the St. Johns CO_2 reservoir.

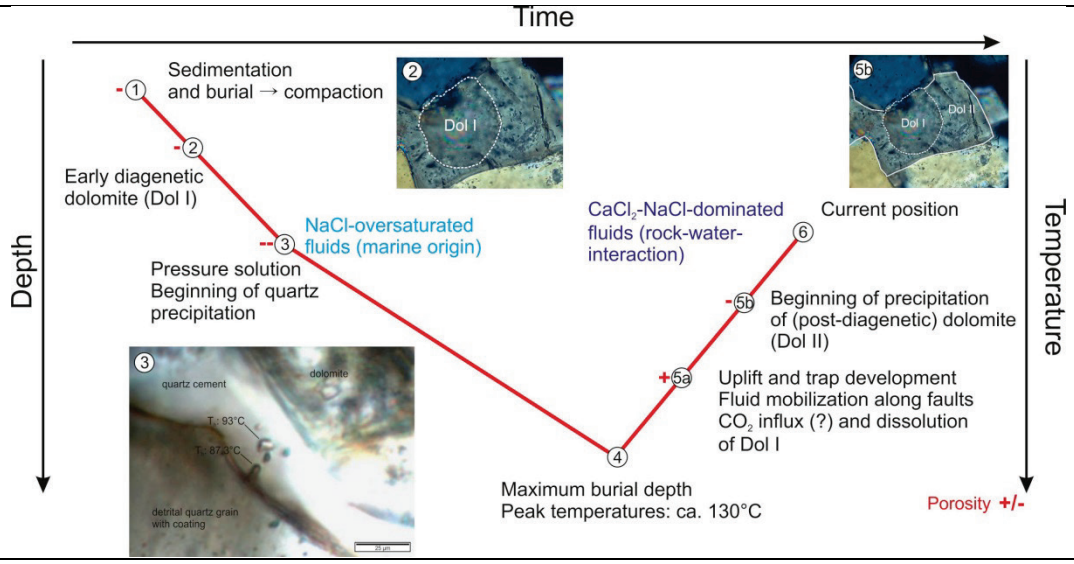

Figure 3: Schematic chronology of the Fizzy Field reservoir showing major events from sedimentation and burial to the current situation after basin inversion.

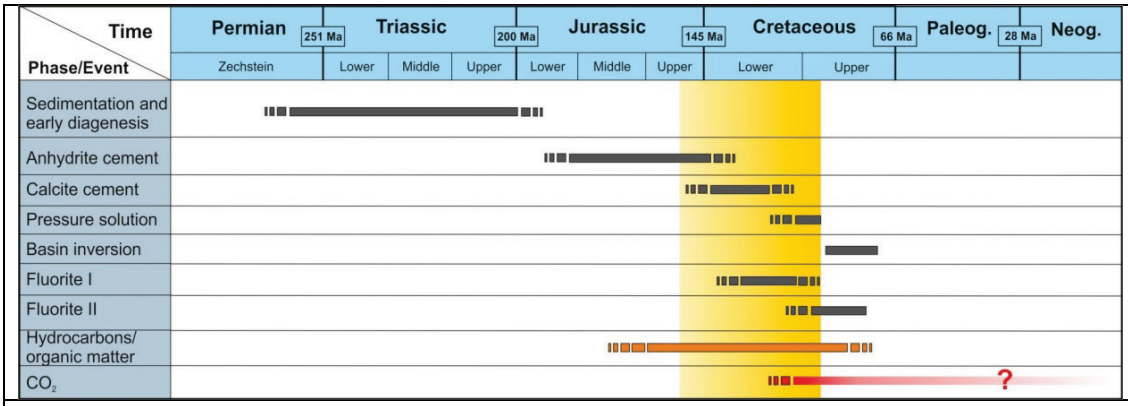

Figure 4: Diagenetic history of the Bahrenborstel site based on microscopic evidence.

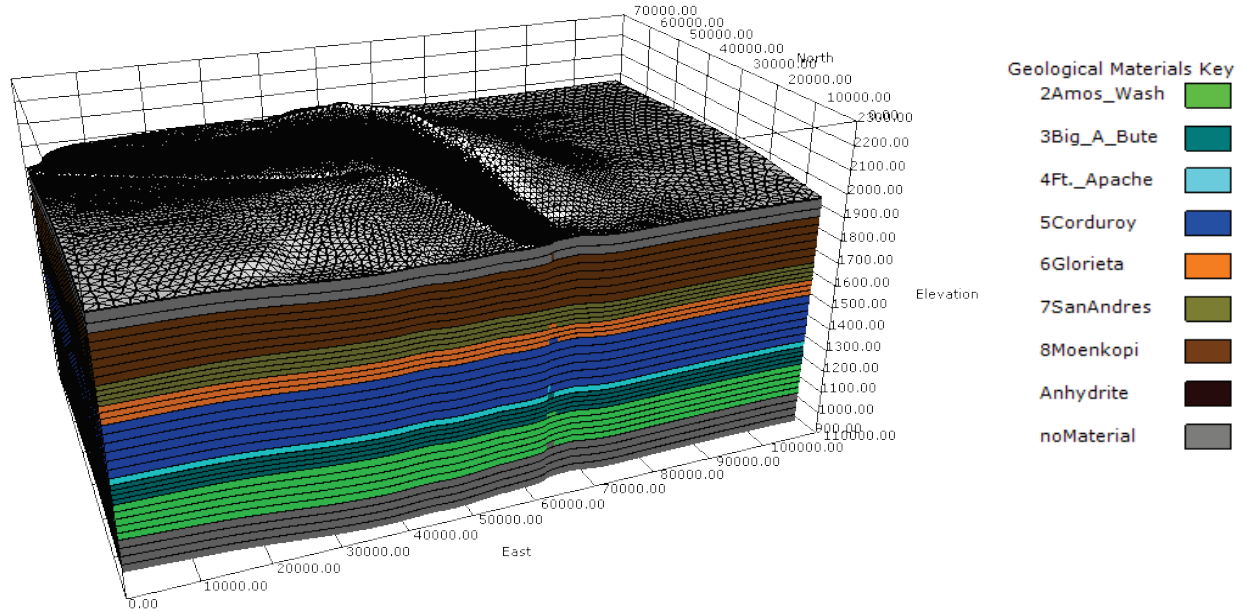

Figure 5: Geologic model of the Saint John reservoir.

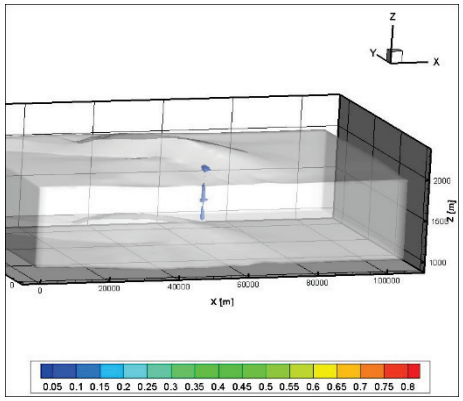	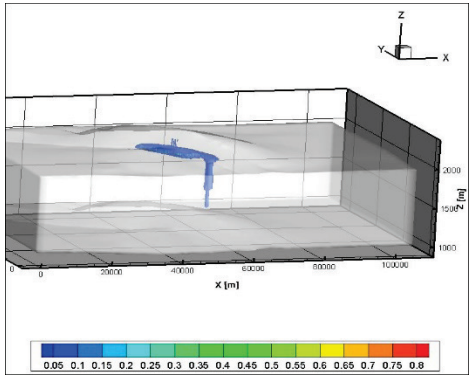	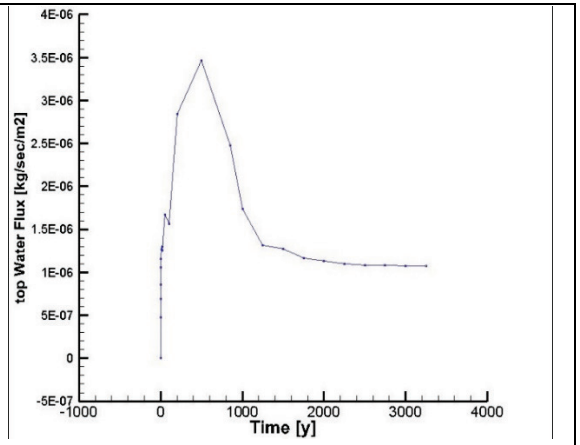
100 years	850 years	Surface flux of brine out of the reservoir through the fault
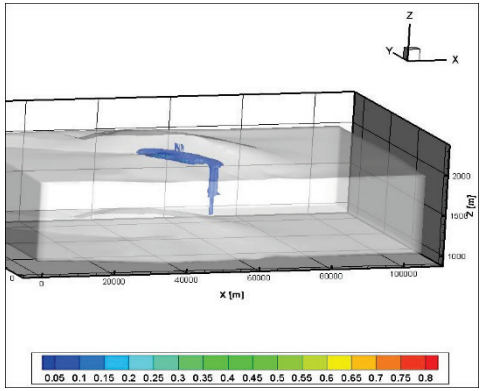	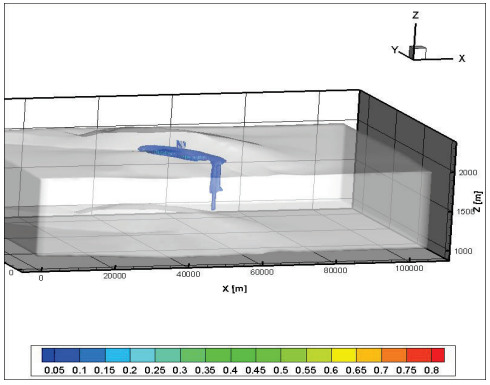	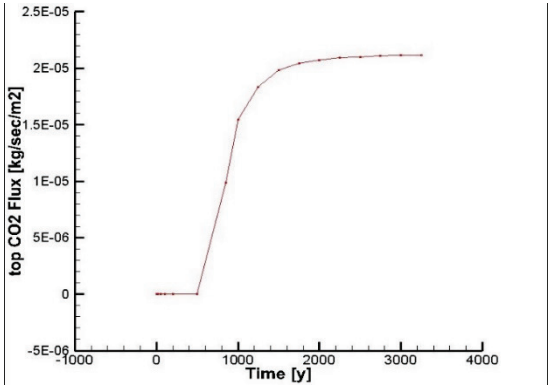
2000 years	3000 years	Surface flux of CO_2 out of the reservoir through the fault

Figure 6: Simulations results of the Saint John analogue reservoir.

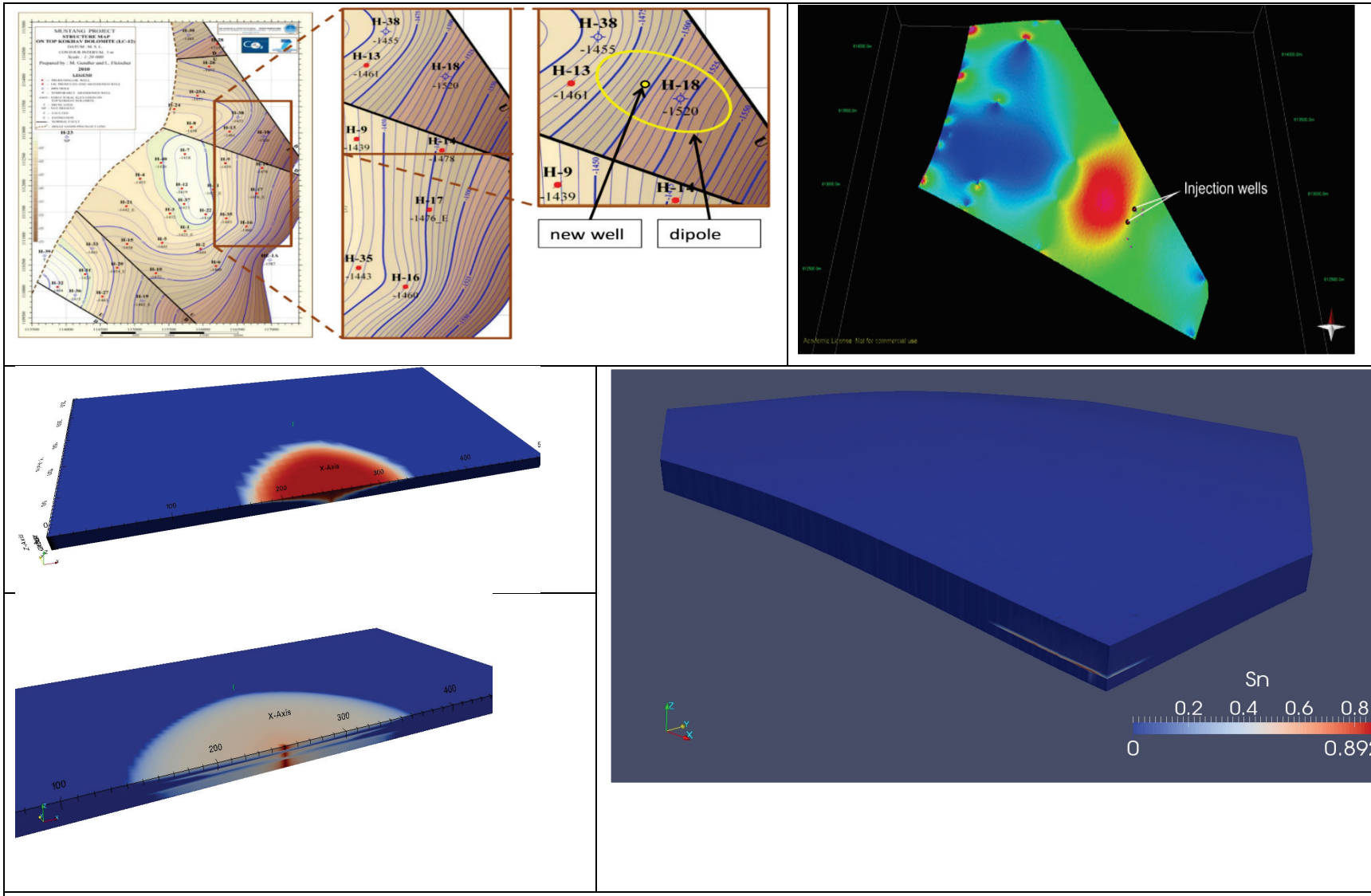

Figure 7: Geomechanical modelling of CO_2 injection at Heletz and map of microfracture generation.

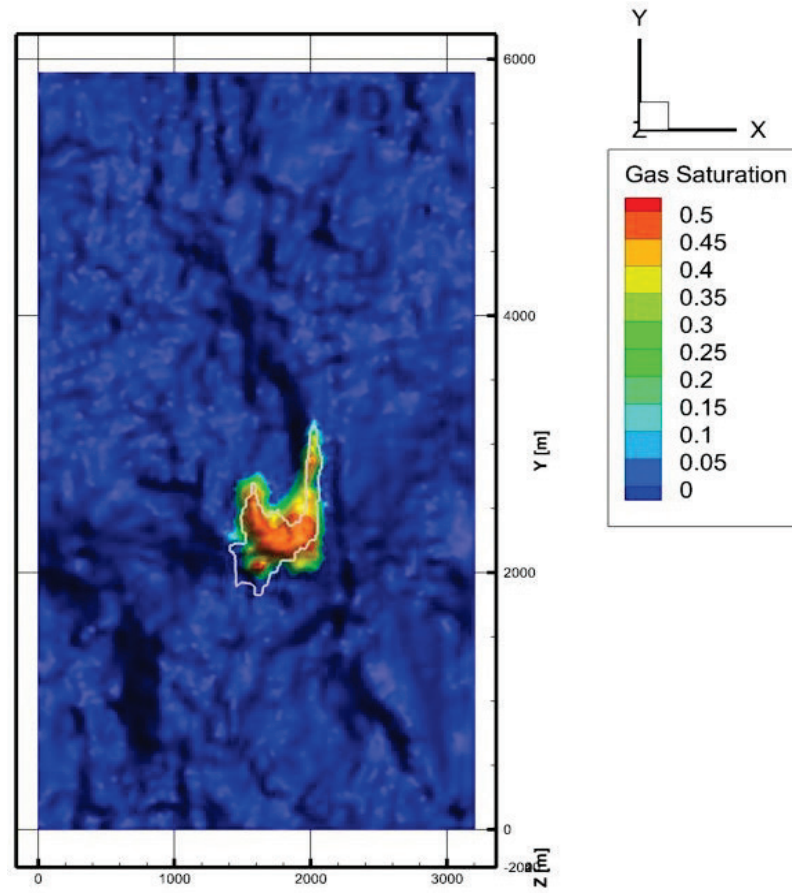

Figure 8: Measured (solid line) and predicted (colour image) CO2 body at Sleipner - 2002.

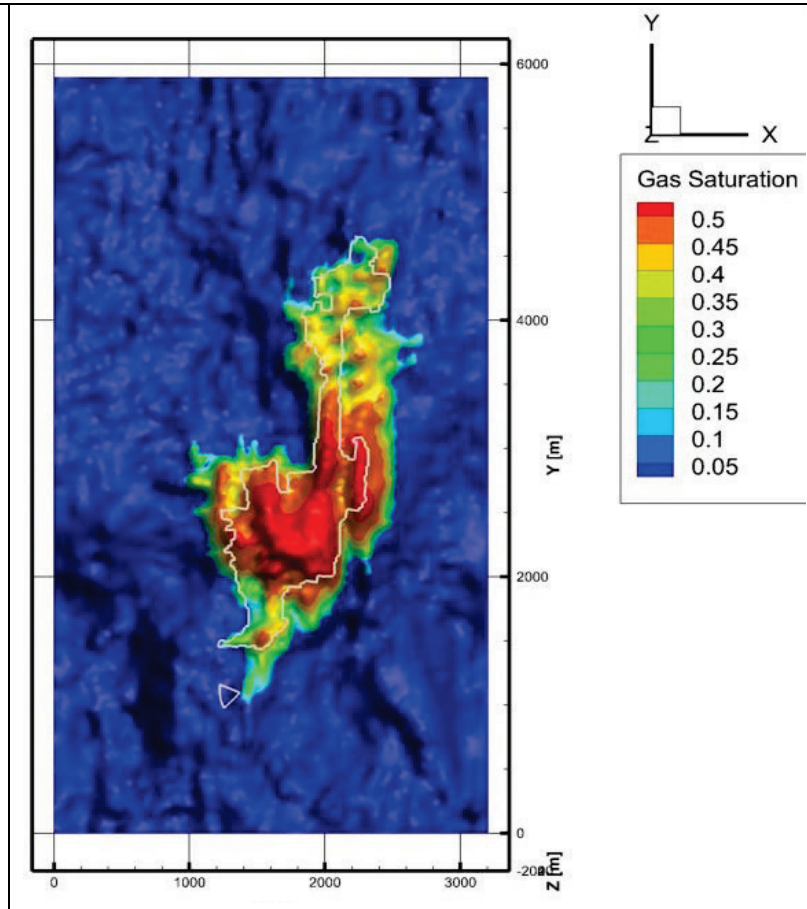

Figure 9: Measured (solid line) and predicted (colour image) CO_2 body at Sleipner - 2008.

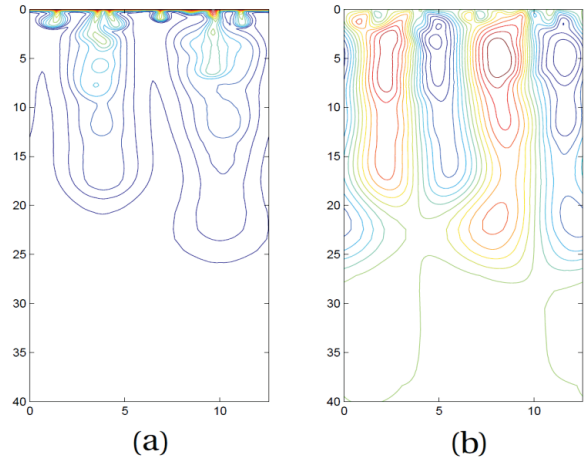

Figure 10: Snapshot of (a) the concentration and (b) the streamfunction f when the system is in a statistically-constant state.

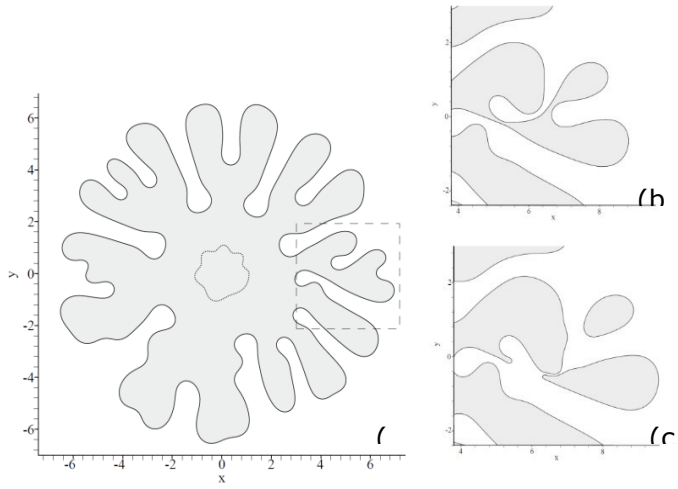

Figure 11: (a) - Asymmetric CO_2 plume (shaded grey) at t = 90, dashed box shows zoomed in areas for (b) and (c). (b) – (c): Zoomed in plots of finger break-off at t = 144 and t = 170 respectively.

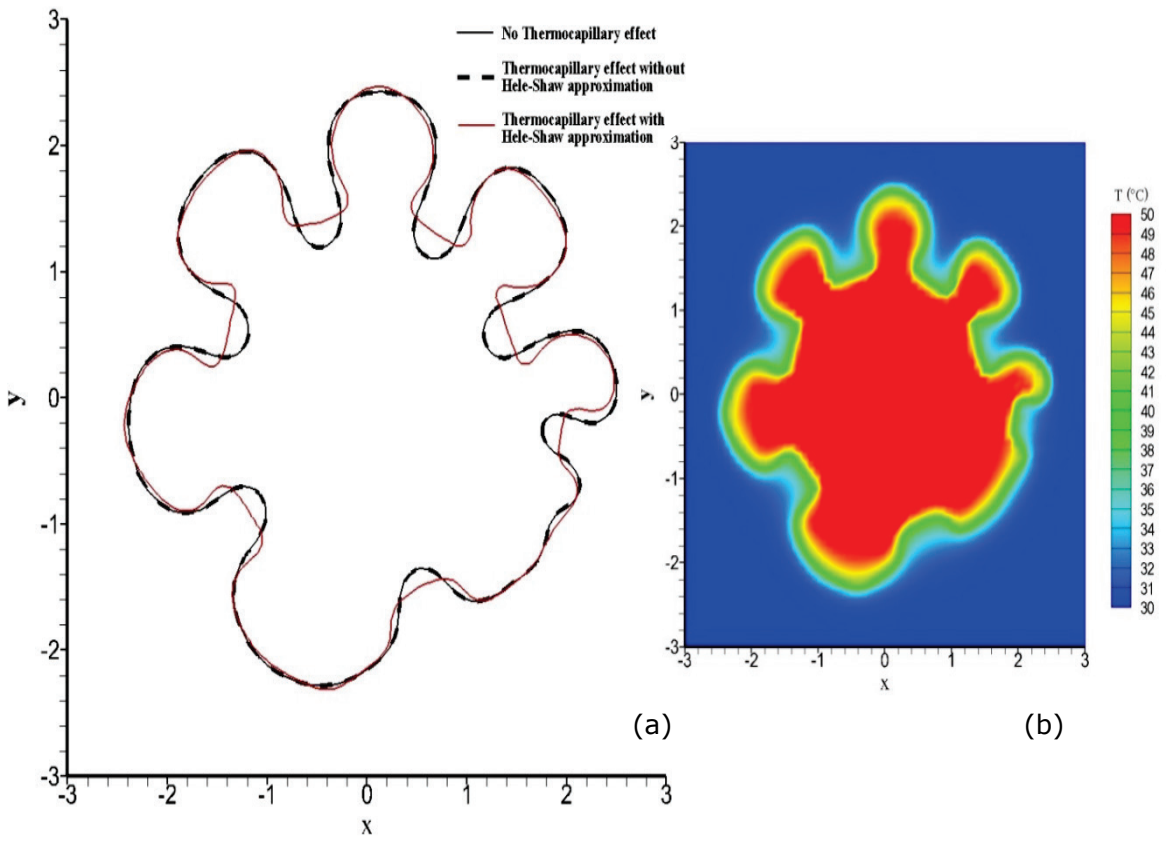

Figure 12: (a) – CO_2 interfaces at t = 10 with varying levels of thermocapillary effects. (b) – Temperature plot for CO_2 injection with thermocapillary effects and Hele-Shaw cell meniscus (red line in (a)) at t = 10.

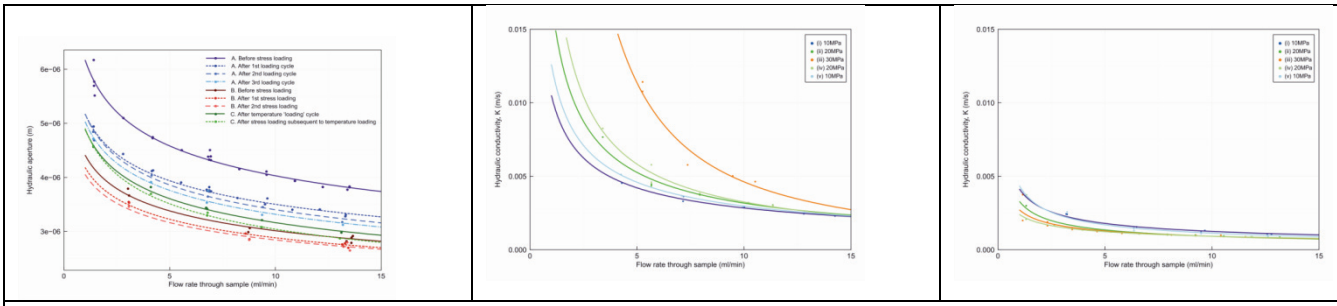

Figure 13: Permeability change as function of the confining pressure.

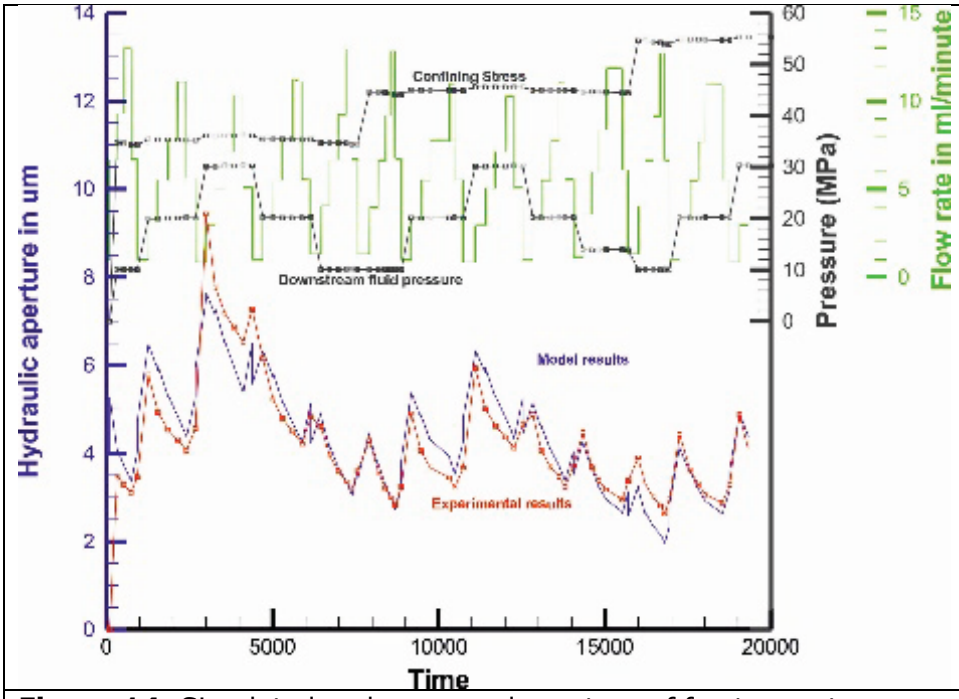

Figure 14: Simulated and measured aperture of fractures at core samples.

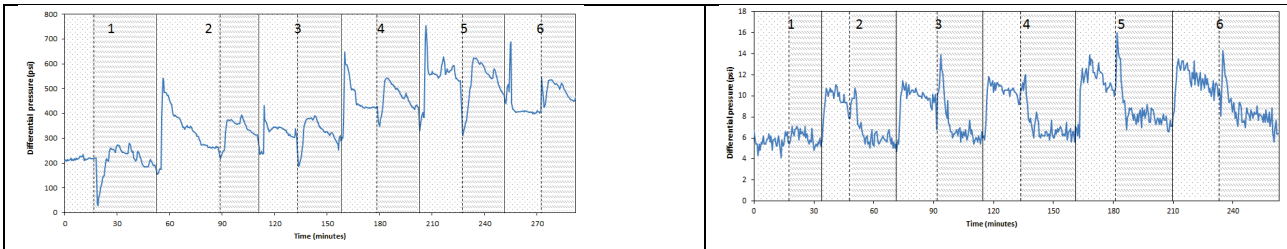

permeable sandstone | fractured caprock

Figure 15: Differential pressure During cyclic phases of scCO2 and then brine/water injection of six water / scCO2 injection cycles.

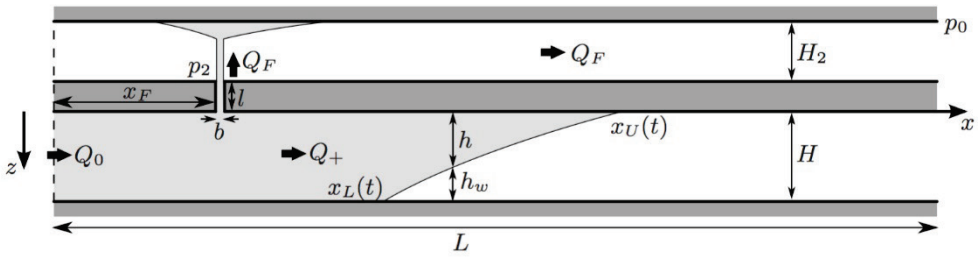

Figure 16: Schematic of leakage geometry from confined aquifers

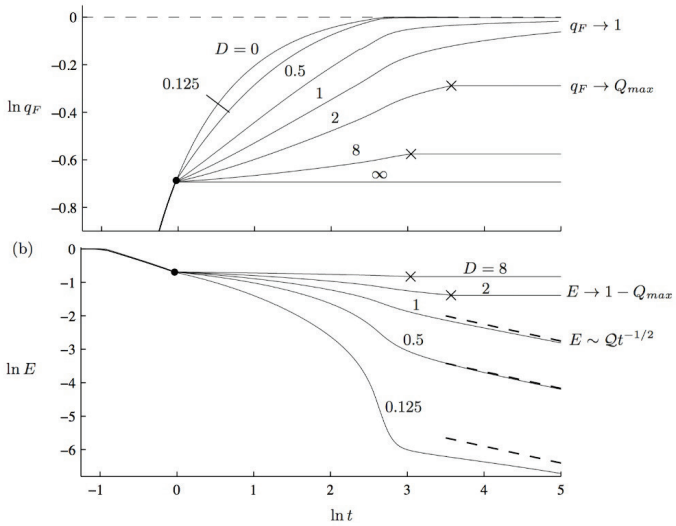

Figure 17: The leakage flux, q_F, and the storage efficiency, E, as a function of time for sample D.

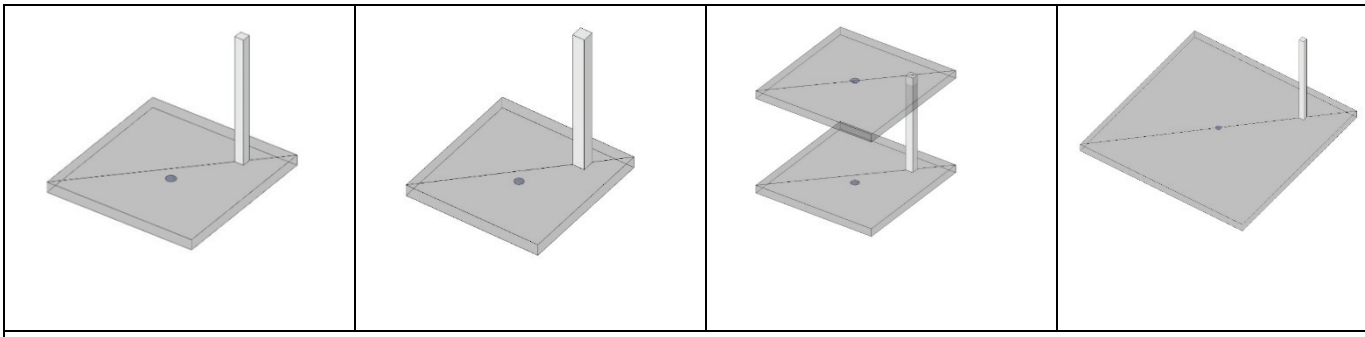

Figure 18: Fault configuration for the quantification of the field-scale leakage.

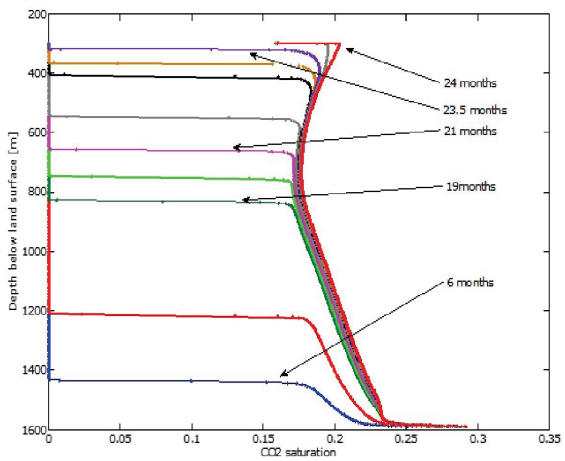

CO_2 saturation pre leakage, 6-24 months (fault k=5.e-13 m^2)

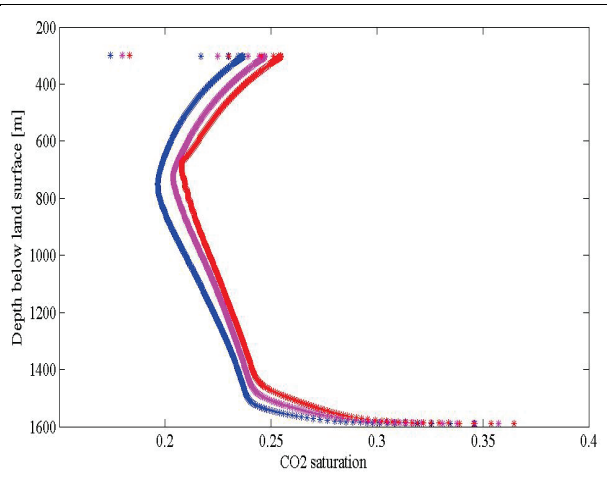

CO_2 saturation during leakage 36-41 months (fault k=8.e-13 m^2)

Figure 19: CO_2 mass fluxes in the fault, before and during breakthrough.

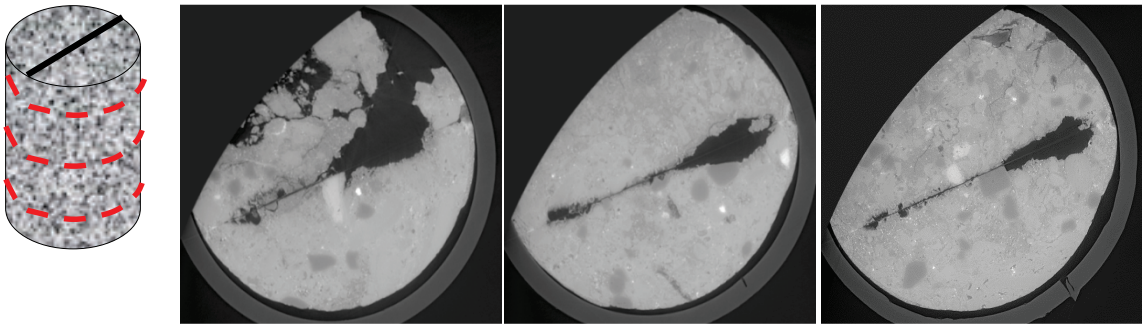

Figure 20: XRMT image cross sections perpendicular to the fracture of the core after the CO_2-enriched brine injection at increasing distance from the inlet (from left to right).

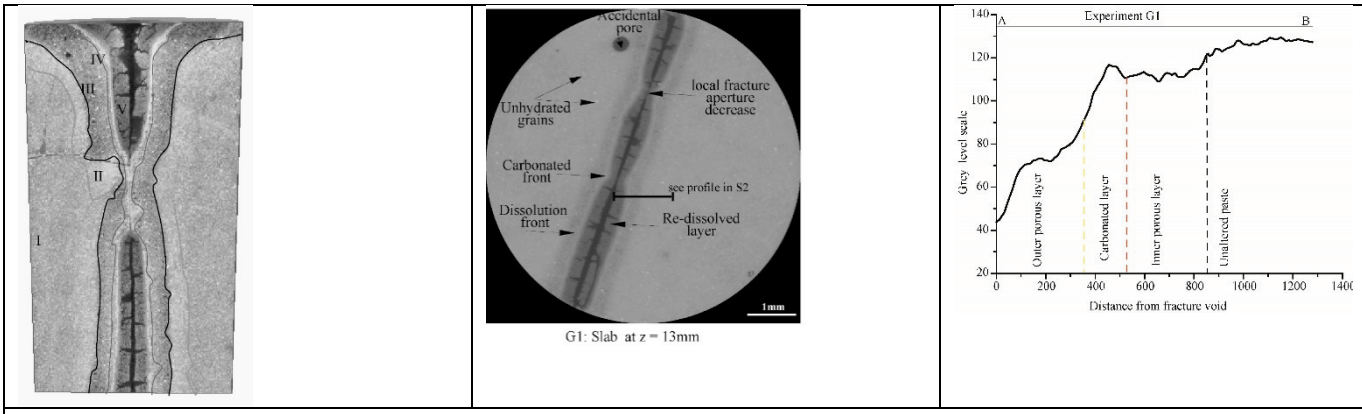

Figure 21: Left: Axial cross section (X-ray tomography) of the sample (sample G3) perpendicular to the initial fracture plane; center and right: sagittal cut with the different alteration zones induced by the CO2 exposure on sample G1.

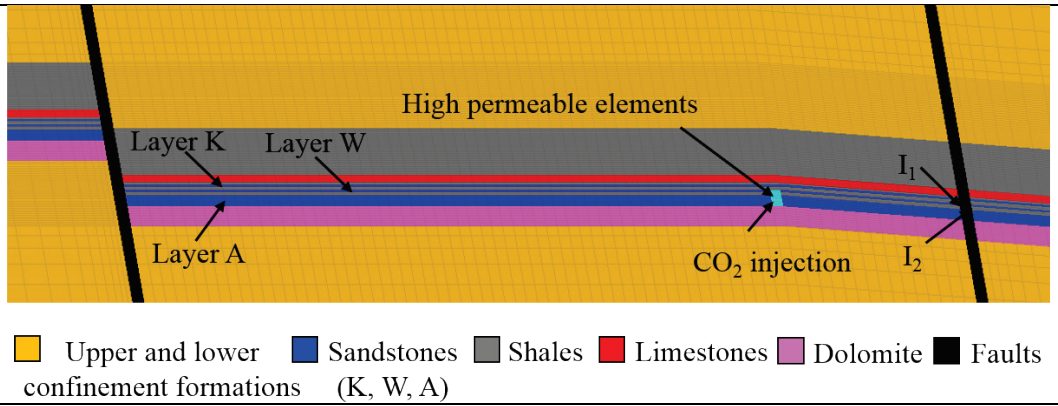

Figure 22: TOUGH-FLAC model to study the hydro-mechanical processes in fault reactivation induced by CO_2 injection in Heletz site

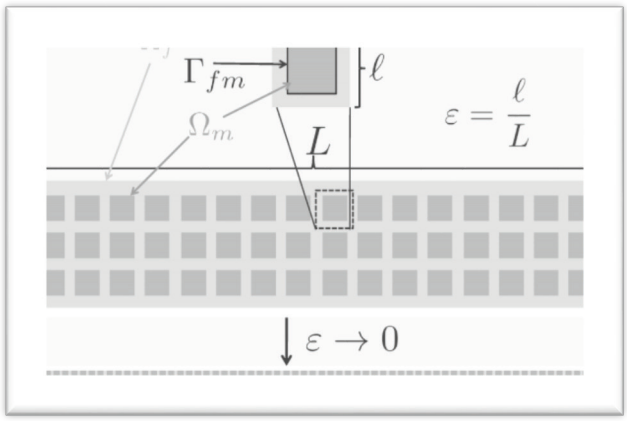

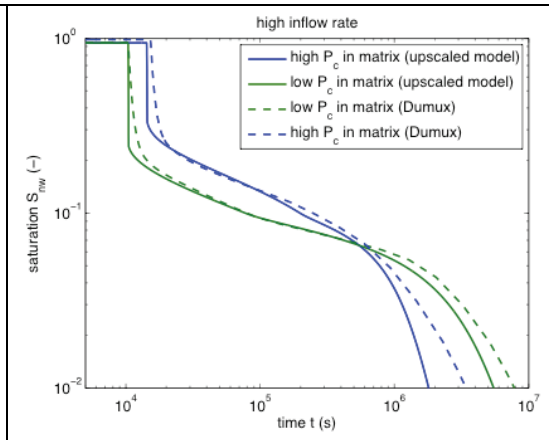

Figure 23: (Left) Sketch of a periodic field with fracture and matrix domain indicated in light gray and dark gray respectively and with the length scales L and `l`. (Right) Saturation of displaced (non-wetting) fluid in the fracture over time for inflow rate.

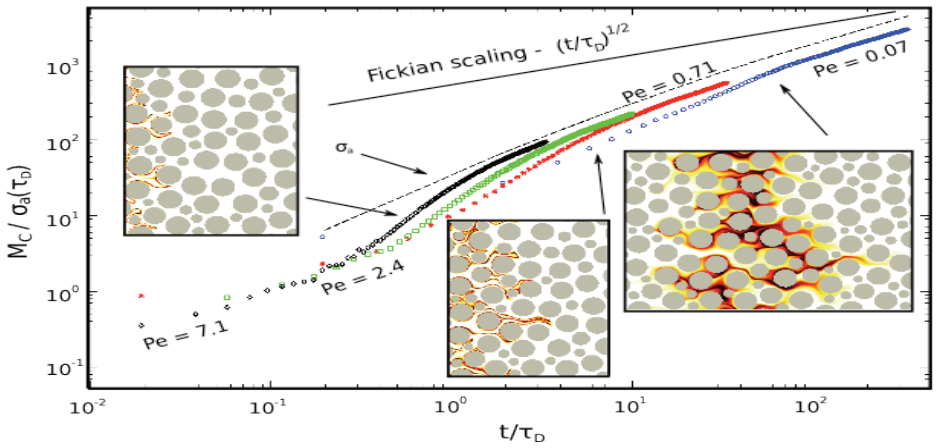

Figure 24: Time evolution of the product mass. The reaction rate is much higher than predicted for a homogeneous medium.

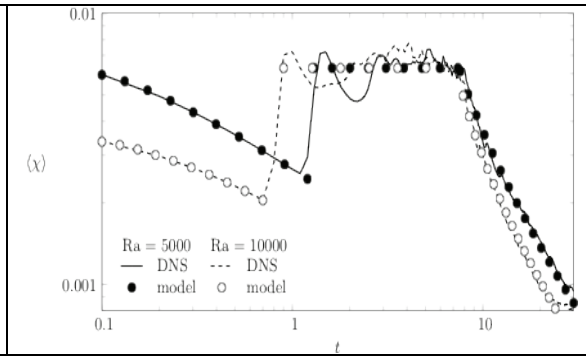

Figure 25: (Left) Mixing ratio, reaction rates and porosity patterns. (Right) Time evolution of the mixing rate.

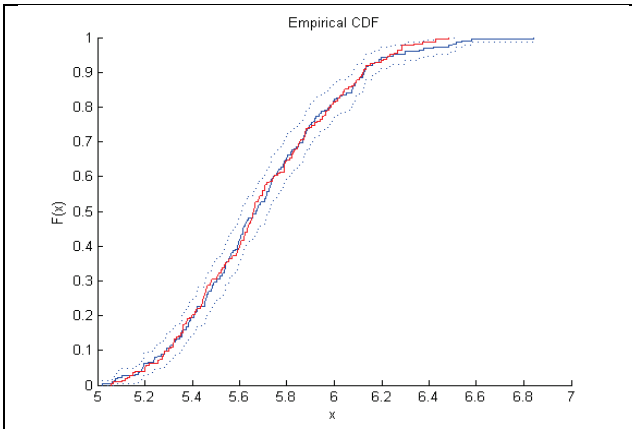

Figure 26: GE (red line) and QMC (black line) distribution functions. The dotted lines shows uncertainty bounds (95% confidence intervals) for the GP Emulator prediction on 225 runs of the porous media model.

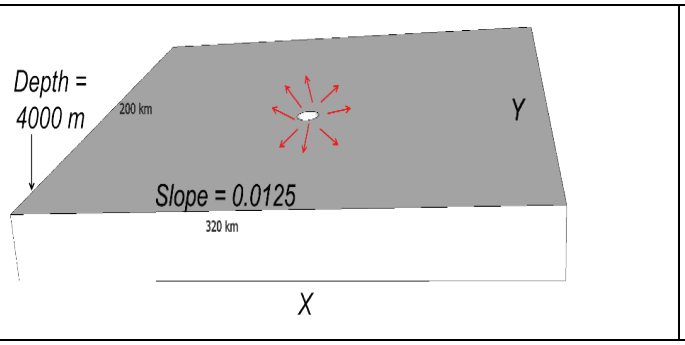

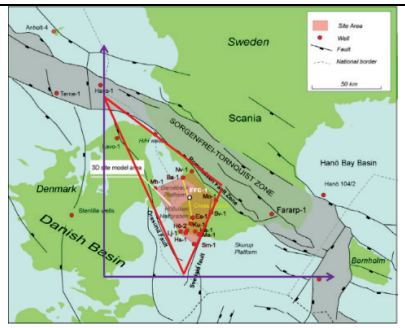

Figure 27: (Left) Schematic of a generic dipping aquifer. (Right) Map of the South Scania site. The red triangle shows the idealised boundaries of the considered reservoir imposed by three faults.

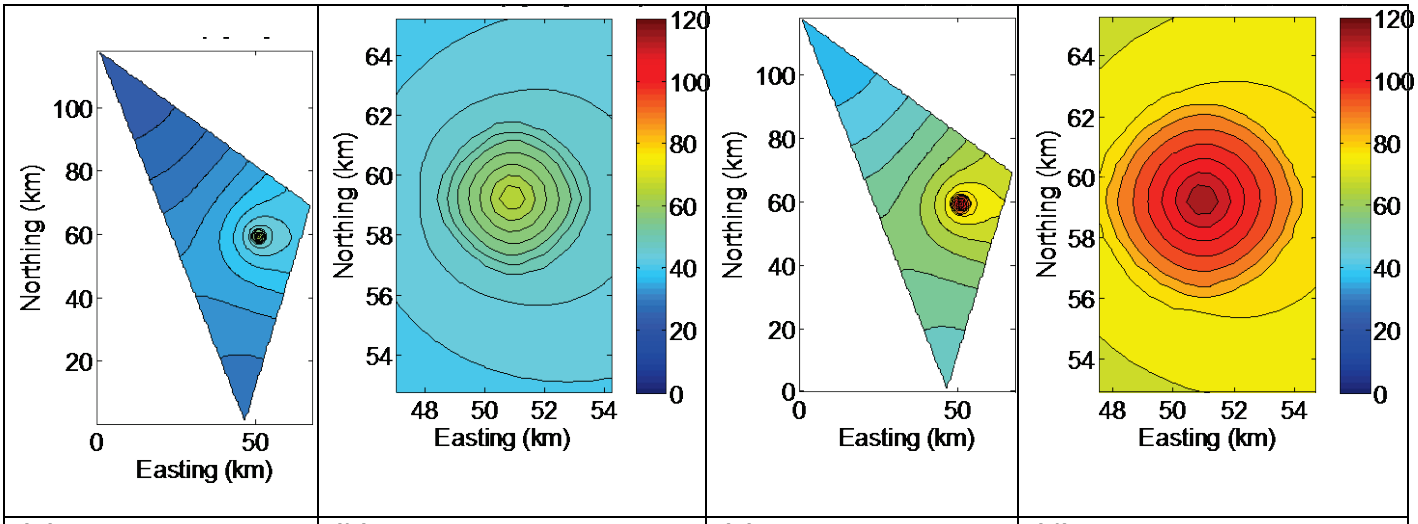

Figure 28: (a) Numerically simulated pressure increase (bar) at 50 years with CO_2 injection rate 1 Mt/yr. (b) Zoom-in view (1 Mt/yr). (c) Numerically simulated pressure increase (bar) with CO_2 injection rate 2 Mt/yr. (b) Zoom-in view (2 Mt/yr).

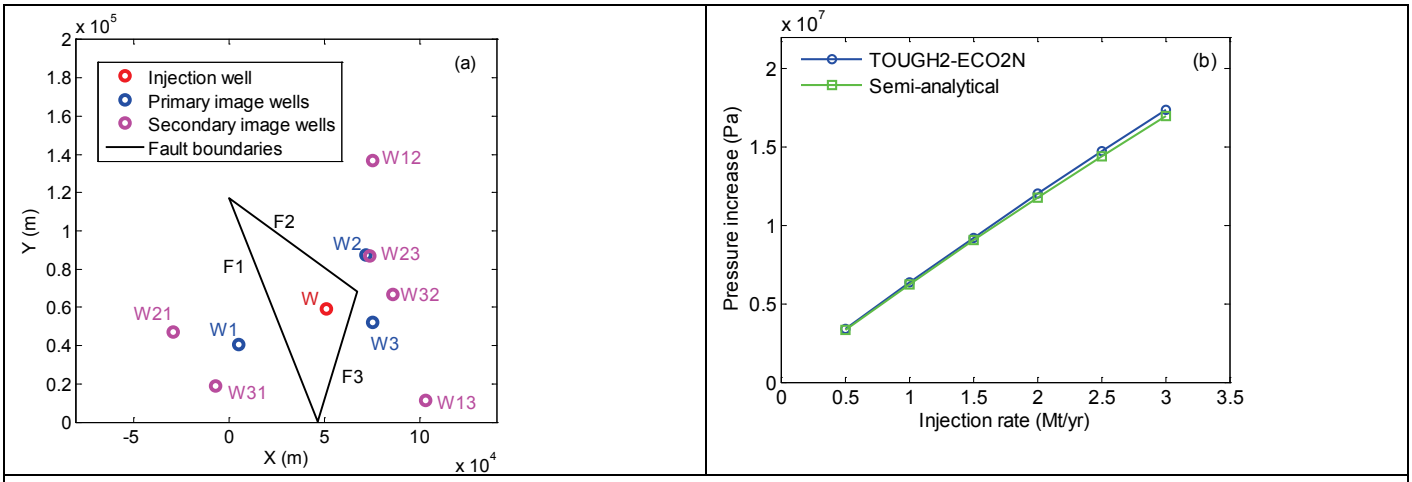

Figure 29: (a) Reservoir modelling domain (Scania site) with fault boundaries and locations of the injection well and image wells. Primary image well W_i is the image of injection well with respect to fault F_i; Secondary image well W_{ij} is the image of primary image well W_i with respect to fault F_j; (b) Comparison of pressure prediction between numerical modeling and analytical solution with superposition of image well solutions.

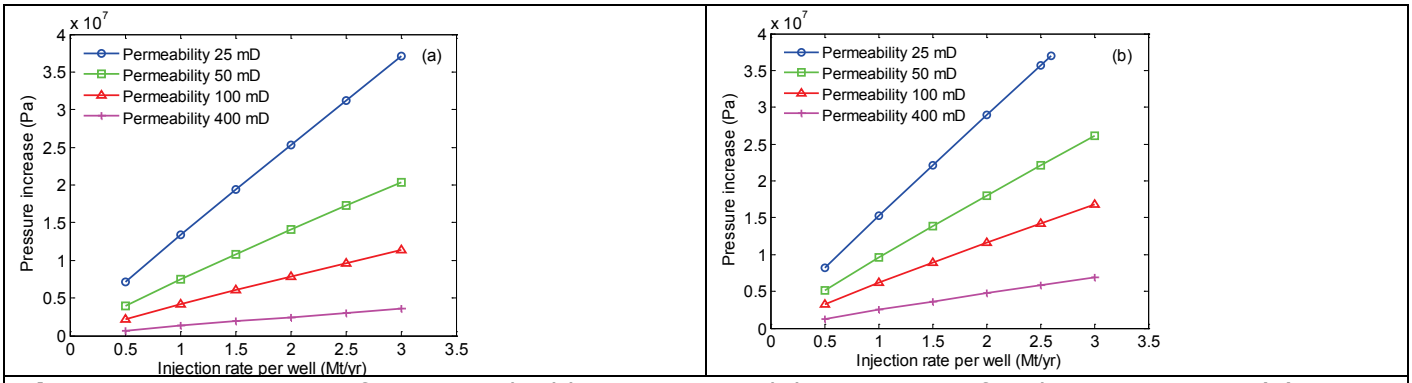

Figure 30: Sensitivity of pressure buildup on permeability variation for the Scania site. (a) Romeleåsen Fault impermeable; (b) all faults impermeable.

Results of CO_2 (non-liquid) Distribution at Different Times	**DuMuX**	**PFLOTRAN**
0.5 Years	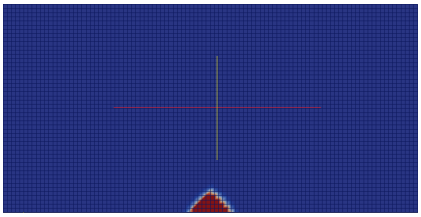	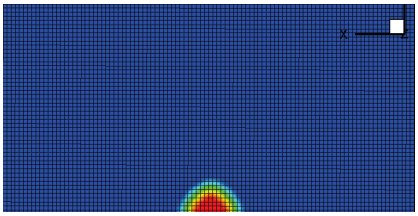
1 Year	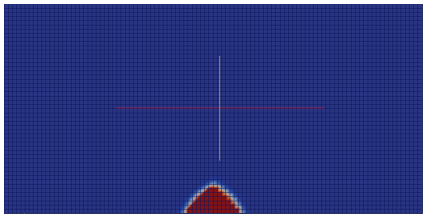	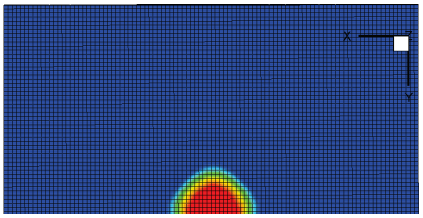
5 Years	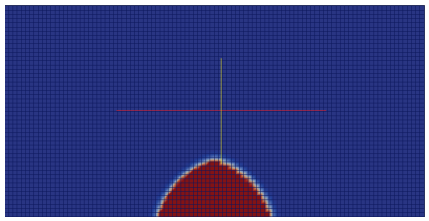	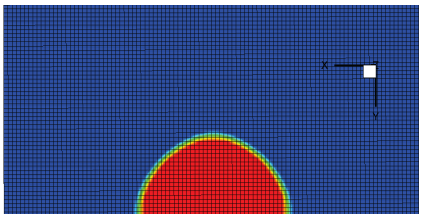
50 Years	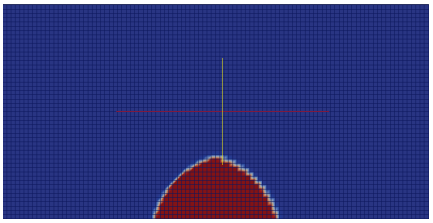	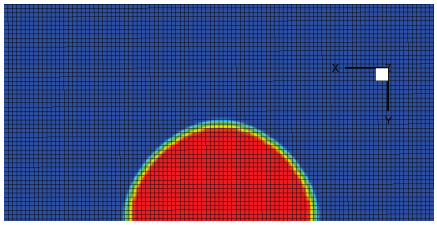

Figure 31: Results of the massively parallel simulations with PFLOTRAN and DUMUX.

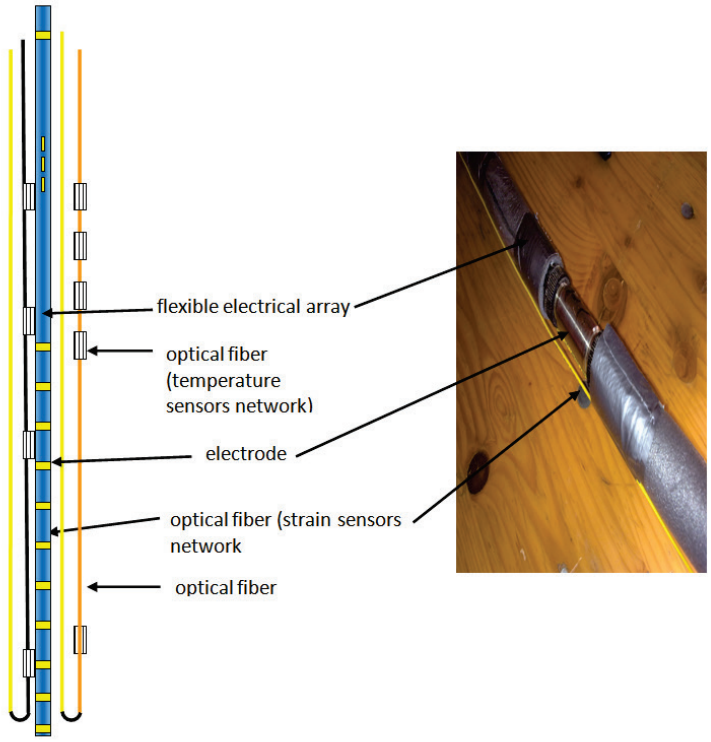

Figure 32: Prototype of the RSTG array.